Polyhedron 225 (2022) 116044

Contents lists available at ScienceDirect

Polyhedron

journal homepage: www.elsevier.com/locate/poly

# Synthesis, characterization and self assembly of dinuclear zinc Schiff base complexes: A combined experimental and theoretical study

Tanmoy Basak [a], Sourav Roy [a,b], Snehasis Banerjee [c], Rosa M. Gomila [d], Antonio Frontera [d,*], Shouvik Chattopadhyay [a,*]

[a] Department of Chemistry, Inorganic Section, Jadavpur University, Kolkata 700032, India
[b] Solid State and Structural Chemistry Unit, Indian Institute of Science, Bangalore 560012, India
[c] Govt. College of Engineering and Leather Technology, Salt Lake Sector-III, Block-LB, Kolkata 700106, India
[d] Department of Chemistry, Universitat de les Illes Baleares, Crta de Valldemossa km 7.5, 07122 Palma de Mallorca (Baleares), Spain

A B S T R A C T

Two new dinuclear zinc(II) complexes, *[(DMSO)Zn($L^1$)Zn(NCS)$_2$]* **(1)** *and [ClZn($L^2$)ZnCl($H_2O$)]•2$CH_3OH$* **(2),** using two different Schiff base ligands, *{$H_2L^1$ = 2,2′-[(2,2-Dimethyl-1,3-propanediyl)bis(nitrilomethylidyne)]bis[4-bromo-6-methoxyphenol]* and *$H_2L^2$ = 2,2′-[(2,2-Dimethyl-1,3-propanediyl)bis(nitrilomethylidyne)]bis[6-ethoxyphenol]},* have been synthesized and characterized by different spectroscopic techniques. The structure guiding non-covalent interactions observed in the solid-state structure of both complexes have been analyzed using DFT calculations, MEP surface analysis, and QTAIM/NCIplot computational tools. The differences in the crystal packing and non-covalent interactions have also been studied using hirshfeld surface analyses and energy frameworks.

## 1. Introduction

Synthesis and the stabilization of supramolecular structures based on coordination compounds could be suitably controlled by the participation of various non-covalent interactions [1–3]. These supramolecular structures have important applications in host–guest chemistry, different sensing applications, and also in catalysis [4–6]. The importance of non-covalent interactions to stabilize a specific conformation of an organic molecule, tertiary and quaternary structures of the proteins and enzymes is also well known [7,8]. The crystal packing is also governed by the suitable interplay of different supramolecular interactions [9–12]. A thorough understanding of these non-covalent interactions is, therefore, of utmost importance to have a good command over several branches of supramolecular chemistry. Employing hydrogen bonds is the most frequently used methodology to design supramolecular structure in complexes [13–15]. Other powerful tools in constructing supramolecular architectures are C—H···π, π···π, cation···π, lone pair···π, and anion···π interactions [16–22]. Apart from hydrogen bond and different π stacking interactions, σ- and π-hole interactions are also important in supramolecular chemistry [23,24].

σ-Hole is a positive electrostatic zone generated along an σ-frame of a species due to the anisotropic distribution of the electron density, whereas, π-holes are the positive electrostatic zones along the perpendicular direction of the σ-frame of a molecule [25]. Calculation of MEP (Molecular Electrostatic Potential) surface could be a very good approach for exploring the σ-holes and/or π-holes in a molecule [26]. They typically interact with an electron-rich centre to generate σ-holes and/or π-holes based interactions. This type of interaction in group 14 elements is termed as tetrel bonding interaction, which is very common for lead(II) complexes [27–29]. Similar interactions involving elements of group 12 are named as spodium bonding [30,31]. Chalcogen bonding (ChB), has been considered a similar type of interaction involving a chalcogen atom and an electron-rich center [32]. The most explored σ-hole based interaction is halogen bonding (HaB), which is an effective tool in modulating supramolecular architectures [33,34].

In this work, we have utilized two $N_2O_2O_2'$ donor Schiff base ligands and designed two dinuclear, *[(DMSO)Zn($L^1$)Zn(NCS)$_2$]* **(1)** and *[ClZn($L^2$)ZnCl($H_2O$)]•2$CH_3OH$* **(2)**, complexes by varying coligands and solvents. In both complexes, the inner zinc(II) centers are pentacoordinated and the outer zinc(II) centers are hexacoordinated. Non-covalent interactions observed in their solid-state structure have been analyzed using DFT calculations, MEP surface analysis, and QTAIM/NCIplot computational tools.

*Abbreviations:* 1, Zinc(II)-Schiff base complex; 2, DFT calculations; 3, Supramolecular assemblies; 4, NCI-Plot.

* Corresponding authors.
*E-mail address:* shouvik.chattopadhyay@jadavpuruniversity.in (S. Chattopadhyay).

https://doi.org/10.1016/j.poly.2022.116044
Received 13 April 2022; Accepted 12 July 2022
Available online 16 July 2022

## 2. Experimental section

All starting materials and solvents were commercially available, reagent grade, and used as purchased from Sigma-Aldrich without further purification.

**Caution!!!** Although no problem was encountered in this work, azide complexes are potentially explosive. Only a small amount of the materials should be prepared and they must be handled with care.

### 2.1. Preparation of ligands

#### 2.1.1. Preparation of $H_2L^1$ and $H_2L^2$

The $N_2O_2O_2'$ donor Schiff base ligands, $H_2L^1$ and $H_2L^2$, were prepared by refluxing 2,2-dimethylpropane-1,3-diamine (1.0 mL, 10 mmol) respectively with 5-bromo-3-methoxysalicylaldehyde (4.80 g, ~20 mmol) and 3-ethoxysalicylaldehyde (3.40 g, ~20 mmol) in methanol solution (10 mL) for ca. 1 h. Yields of both ligands are around 8 mmol and they were not isolated but used directly for the preparation of complexes **1** and **2**, respectively.

### 2.2. Preparation of complexes

#### 2.2.1. [(DMSO)Zn($L^1$)Zn(NCS)$_2$] (1)

A methanol solution (50 mL) of zinc(II) acetate dihydrate (4.40 g, ~20 mmol) was added to the methanol solution of the ligand, $H_2L^1$ and the resulting solution was refluxed for ca. 1 h. A methanol–water (2:1) solution (25 mL) of sodium thiocyanate (1.30 g, ~20 mmol) was added and the refluxing was continued for an additional hour. Little turbidity arises in the solution and 5 mL DMSO was then added to obtain a clear solution. It was kept in an open atmosphere for a few days to get crystals of complex **1**. Suitable single crystals for X-ray diffraction were collected from this product.

**Yield:** 5.95 g (~70 %) based on zinc(II). Colour: Yellow; Anal. Calc. for $C_{25}H_{28}Br_2N_4O_5S_3Zn_2$ (FW 851.30): C, 35.27; H, 3.32; N, 6.58; Found: C, 35.2; H, 3.3; N, 6.6 %. IR (KBr, cm$^{-1}$): 1626 ($\nu_{C=N}$), 2088 ($\nu_{NCS}$), 2845–2965 ($\nu_{C-H}$). UV–Vis, $\lambda^{max}$ (nm), [$\varepsilon_{max}$ (L mol$^{-1}$ cm$^{-1}$)] (DMSO): 232 (7.8 × 10$^3$), 270 (5.2 × 10$^3$), 356 (2.7 × 10$^3$).

#### 2.2.2. [ClZn($L^2$)ZnCl($H_2O$)]•2$CH_3OH$ (2)

A methanol solution (50 mL) of zinc(II) acetate dihydrate (4.40 g, ~20 mmol) was added to the methanol solution of the ligand, $H_2L^2$ and the resulting solution was refluxed for ca. 1 h. A methanol–water (2:1) solution (25 mL) of potassium chloride (1.30 g, ~20 mmol) was added and it was refluxed for an additional hour. It was then cooled to room temperature and kept undisturbed in an open atmosphere. Crystals of complex **2** were obtained after a few days. X-ray diffraction quality single crystals were collected from this product.

**Yield:** 4.62 g (~68 %) based on zinc(II). Colour: Yellow; Anal. Calc. for $C_{25}H_{38}Cl_2N_2O_7Zn_2$ (FW 680.25): C, 44.83; H, 4.91; N, 4.55; Found: C, 44.8; H, 4.9; N, 4.6 %. IR (KBr, cm$^{-1}$): 1626 ($\nu_{C=N}$), 2889–2997 ($\nu_{C-H}$), 3351–3407 ($\nu_{O-H}$). UV–Vis, $\lambda^{max}$ (nm), [$\varepsilon_{max}$ (L mol$^{-1}$ cm$^{-1}$)] (DMSO): 232 (8.0 × 10$^3$), 270 (6.2 × 10$^3$), 356 (2.5 × 10$^3$).

### 2.3. Physical measurement

A PerkinElmer 240C elemental analyzer has been used to get the data of elemental analysis (carbon, hydrogen, and nitrogen). A PerkinElmer FTIR Spectrum Two spectrophotometer has been used to run IR spectra (4500–500 cm$^{-1}$). A Shimadzu UV-1700 UV–vis spectrophotometer has been used to record the electronic spectra in DMSO.

### 2.4. X-ray crystallography

Suitable single crystals of both complexes were picked out and mounted on a glass fiber. A 'Bruker D8 QUEST area detector' diffractometer equipped with graphite-monochromated Mo $K_\alpha$ radiation ($\lambda$ = 0.71073 Å) has been used for X-ray data collection. A direct method has been used to solve the structures and refinement has been done by full-matrix least-squares on $F^2$ using the SHELX-18 package [35]. The hydrogen atoms, attached to the oxygen atoms of coordinated water and non-coordinated methanol were located by difference Fourier maps and were kept at fixed positions. Non-hydrogen atoms were refined with anisotropic thermal parameters. All other hydrogen atoms were placed in their geometrically idealized positions and constrained to ride on their parent atoms. Multi-scan empirical absorption corrections were applied to the data using the program SADABS [36]. Table 1 gathers the crystallographic data and refinement details of both complexes. Important bond lengths and angles are listed in Tables 2 and 3, respectively.

**Table 1**
Crystal data and refinement details of complexes **1** and **2**.

| Complex | 1 | 2 |
|---|---|---|
| Formula | $C_{25}H_{28}Br_2N_4O_5S_3Zn_2$ | $C_{25}H_{38}Cl_2N_2O_7Zn_2$ |
| Formula Weight | 851.27 | 680.25 |
| Temperature (K) | 293 | 293 |
| Crystal System | Monoclinic | Monoclinic |
| Space group | $P2_1/n$ | $P2_1/c$ |
| $a$ (Å) | 12.1465(14) | 14.010(8) |
| $b$ (Å) | 21.648(3) | 13.782(6) |
| $c$ (Å) | 13.0065(16) | 16.451(9) |
| α () | 90 | 90 |
| β () | 90.506(4) | 108.39(3) |
| γ () | 90 | 90 |
| Z | 4 | 4 |
| $d_{cal}$ (g cm$^{-3}$) | 1.653 | 1.499 |
| μ(mm$^{-1}$) | 3.961 | 1.812 |
| F(000) | 1696 | 1408 |
| Total reflection | 59,209 | 56,830 |
| Unique Reflections | 7087 | 6655 |
| Observed data [I > 2σ(I)] | 3751 | 5570 |
| R(int) | 0.098 | 0.055 |
| R1, w$R2$ (all data) | 0.1377, 0.1999 | 0.0435, 0.0879 |
| R1, w$R2$ [I > 2σ (I)] | 0.0677, 0.1581 | 0.0330, 0.0815 |
| GOF | 1.008 | 1.058 |
| CCDC Number | 2,036,440 | 2,036,441 |

**Table 2**
Selected bond lengths (Å) of complexes **1** and **2**.

| Complex | 1 | 2 |
|---|---|---|
| Zn(1) – O(1) | 2.045(6) | 2.063(2) |
| Zn(1) – O(2) | 2.052(6) | 2.060(2) |
| Zn(1) – N(1) | 2.047(7) | 2.104(3) |
| Zn(1) – N(2) | 2.058(7) | 2.062(3) |
| Zn(2) – O(1) | 2.035(6) | 2.015(3) |
| Zn(2) – O(2) | 2.025(6) | 2.018(2) |
| Zn(2) – O(3) | 2.541(6) | 2.593(3) |
| Zn(2) – O(4) | 2.676(6) | 2.577(3) |
| Zn(2) – N(3) | 1.930(9) | – |
| Zn(2) – N(4) | 1.915(9) | – |
| Zn(1) – O(5) | 2.020(7) | – |
| Zn(2) – O(7) | – | 1.994(3) |
| Zn(1) – Cl(1) | – | 2.2872(17) |
| Zn(2) – Cl(2) | – | 2.2230(18) |

### 2.5. Theoretical methods

The calculations of both complexes studied herein were performed at the PBE0 [37]-D3 [38]/def2-TZVP [39] level of theory using Gaussian-16 program [40]. The MEP surfaces have been constructed using the 0.001 a.u. isosurface as estimate of the van der Waals surface at the same level of theory. The Bader's Quantum Theory of "atoms-in-molecules" (QTAIM)[41] in combination with the non-covalent interaction plot (NCIplot) index [42] were used to characterize the interactions by musing MULTIWFN program [43]. The QTAIM/NCIPlot representations

**Table 3**
Selected bond angles (°) of complexes **1** and **2**.

| Complex | 1 | 2 |
|---|---|---|
| Cl(1)-Zn(1)-O(1) | | 104.64(8) |
| Cl(1)-Zn(1)-O(2) | | 109.02(8) |
| Cl(1)-Zn(1)-N(1) | | 102.48(8) |
| Cl(1)-Zn(1)-N(2) | | 106.15(8) |
| O(1)-Zn(1)-O(2) | 75.7(2) | 75.40(9) |
| O(1)-Zn(1)-O(5) | 104.0(3) | |
| O(1)-Zn(1)-N(1) | 90.0(2) | 87.15(10) |
| O(1)-Zn(1)-N(2) | 150.7(3) | 148.27(10) |
| O(2)-Zn(1)-O(5) | 99.0(3) | |
| O(2)-Zn(1)-N(1) | 158.5(3) | 146.88(10) |
| O(2)-Zn(1)-N(2) | 89.9(3) | 87.46(10) |
| O(5)-Zn(1)-N(1) | 100.0(3) | |
| O(5)-Zn(1)-N(2) | 103.4(3) | |
| N(1)-Zn(1)-N(2) | 95.5(3) | 93.55(11) |
| Cl(2)-Zn(2)-O(1) | | 114.36(8) |
| Cl(2)-Zn(2)-O(2) | | 116.10(8) |
| Cl(2)-Zn(2)-O(3) | | 87.52(7) |
| Cl(2)-Zn(2)-O(4) | | 84.79(7) |
| Cl(2)-Zn(2)-O(7) | | 129.98(9) |
| O(1)-Zn(2)-O(2) | 76.5(2) | 77.38(9) |
| O(1)-Zn(2)-O(3) | 68.1(2) | 67.79(9) |
| O(1)-Zn(2)-O(4) | 142.3(2) | 145.28(9) |
| O(1)-Zn(2)-O(7) | | 104.55(11) |
| O(1)-Zn(2)-N(3) | 113.3(3) | |
| O(1)-Zn(2)-N(4) | 114.8(3) | |
| O(2)-Zn(2)-O(3) | 144.5(2) | 143.95(9) |
| O(2)-Zn(2)-O(4) | 66.4(2) | 68.05(8) |
| O(2)-Zn(2)-N(3) | 109.8(4) | |
| O(2)-Zn(2)-N(4) | 113.9(3) | |
| O(2)-Zn(2)-O(7) | | 101.73(11) |
| O(3)-Zn(2)-O(4) | 148.1(2) | 145.11(8) |
| O(3)-Zn(2)-O(7) | | 79.04(10) |
| O(4)-Zn(2)-O(7) | | 80.12(9) |
| O(3)-Zn(2)-N(3) | 86.9(3) | |
| O(3)-Zn(2)-N(4) | 80.4(3) | |
| O(4)-Zn(2)-N(3) | 86.3(3) | |
| O(4)-Zn(2)-N(4) | 76.4(3) | |
| N(3)-Zn(2)-N(4) | 120.4(4) | |

were generated using VMD software [44].

### 2.6. Hirshfeld surface analysis

Hirshfeld surfaces [45] were established by electron distribution and obtained as the sum of the electron densities of spherical atoms [46]. Hirshfeld surfaces are useful in analyzing properties of short/long contacts of non-covalent interactions through color-coding in the crystal lattice. A particular Hirshfeld surface is obtained for specified crystal and spherical atomic densities [47]. The Hirshfeld surfaces and 2D fingerprint plots were calculated with the help of Crystal Explorer 17.5 [48]. The normalized contact distance ($d_{norm}$) is determined by the distance of the atom inside ($d_i$) and outside ($d_e$) to the Hirshfeld surface with the vdW radii of the corresponding atom [49]. The 2D fingerprint plot displayed brief information on intermolecular contacts through a combination of $d_e$ and $d_i$ in the crystal [50].

## 3. Results and discussion

### 3.1. Synthesis

In the present work, two $N_2O_2O_2'$ donors compartmental Schiff base ligands, $H_2L^1$ *and* $H_2L^2$, were synthesized by the condensation of 2,2-dimethylpropane-1,3-diamine with 5-bromo-2-hydroxy-3-methoxysalicylaldehyde and 3-ethoxysalicylaldehyde, respectively following the literature method [51]. The ligands were not isolated and purified, but used *in situ* for the preparation of both zinc(II) complexes. The reaction of the ligand, $H_2L^1$, with zinc(II) acetate in presence of sodium thiocyanate in a 1:2:2 ratios in DMSO produces complex **1**. On the other hand, the reaction of the ligand, $H_2L^2$ with zinc(II) acetate in the presence of potassium chloride in appropriate solvent (methanol) in same ratio produces complex **2**. Complexes **1** and **2** are simple dinuclear complexes. Both the inner and outer compartments of both ligands are occupied by zinc(II) centers. The formation of both complexes is shown in Scheme 1.

### 3.2. Description of structures

#### 3.2.1. [(DMSO)Zn($L^1$)Zn(NCS)$_2$] (1) and [ClZn($L^2$)ZnCl($H_2O$)]•2$CH_3OH$ (2)

Single crystal X-ray diffraction analyses reveal that both complexes crystallize in monoclinic space groups (Table 1). Both Schiff base ligands, $H_2L^1$ and $H_2L^2$, are $N_2O_2O_2'$ donor compartmental Schiff bases having inner $N_2O_2$ and outer $O_2O_2'$ compartments where both the compartments are occupied by zinc(II) centres. The asymmetric unit of complex **2** contains two non-coordinated methanol as lattice solvent molecules. Perspective views of complexes **1** and **2** are shown in Fig. 1.

In both complexes **1** and **2**, the penta-coordinated zinc(II) center, Zn (1), residing in the inner $N_2O_2$ compartment, has distorted square pyramidal geometry with $\tau = 0.13$ and 0.02 respectively [$\tau$ = Addison parameter[52] = $(a - b)/60$, where $a$ and $b$ are the two largest Ligand–Metal–Ligand angles in the coordination sphere], in which two imine nitrogen atoms, N(1) and N(2), and two phenoxo oxygen atoms, O (1) and O(2), of the deprotonated di-Schiff base constitute the equatorial plane. An oxygen atom, O(5), from a DMSO molecule is coordinated in the axial position of zinc(II) in complex **1**, whereas in complex **2**, the axial position is coordinated by a chloride ion, Cl(1). The trans angles N

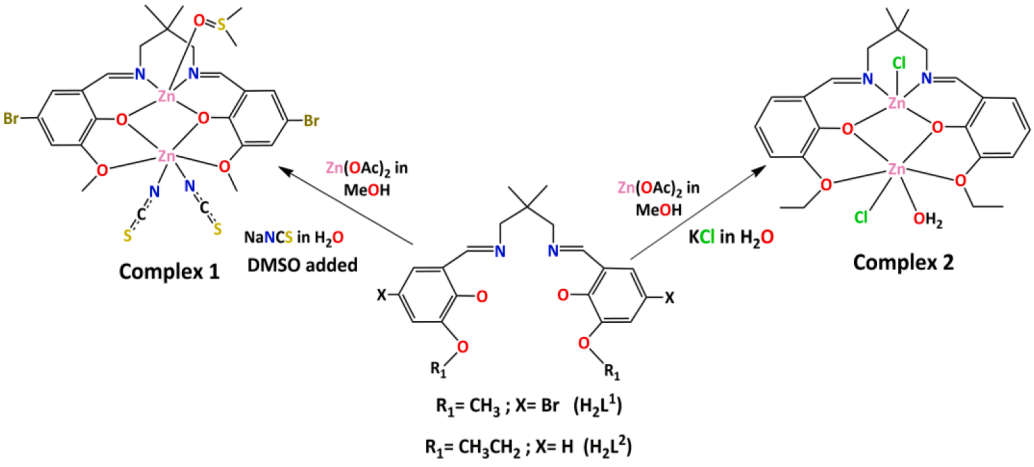


**Scheme 1.** Synthesis of complexes **1** and **2**.

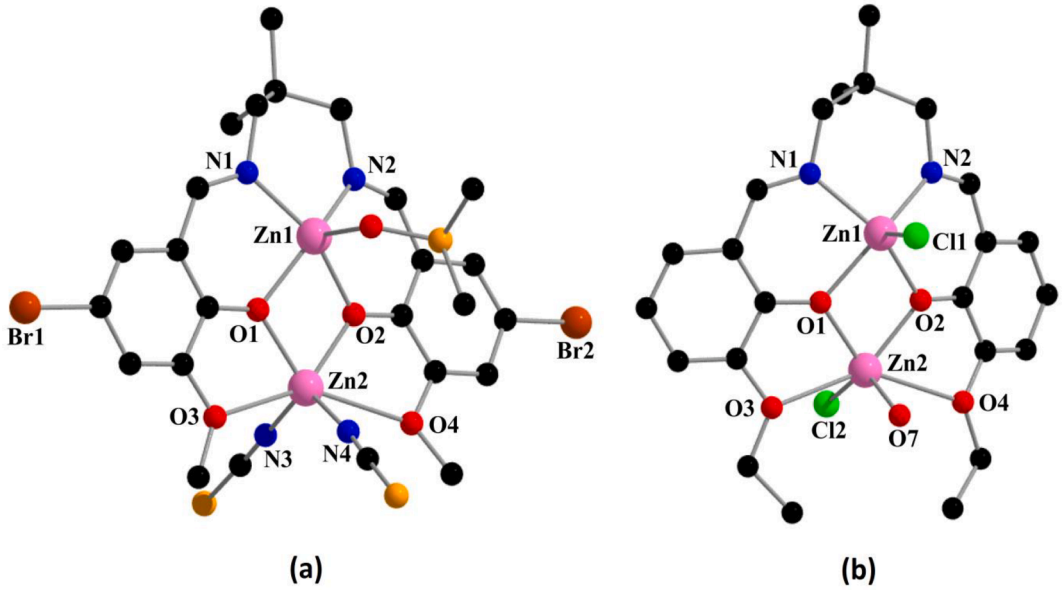


**Fig. 1.** Perspective views of complexes **1** (**a**) and **2** (**b**) with selective atom numbering scheme. Hydrogen atoms and lattice solvent molecules have been omitted for clarity.

(1)-Zn(1)-O(2), N(2)-Zn(1)-O(1) [around Zn(1)] are found to be ~ 158.4 (3)°, 150.7(3)° and 146.9(1)°, 148.27(9)° in complexes **1** and **2** respectively. Now, these XZnL′ [where L′= $L^1$ and $L^2$, X = DMSO or Cl] moieties can act as metalloligands and, another zinc(II) is trapped in the $O_2O_2'$ compartments. The zinc(II) centers, Zn(2), in the outer $O_2O_2'$ compartments, have distorted octahedral geometries. In both complexes, Zn(2), is coordinated by two phenoxy oxygen atoms, O(1) and O(2), and two methoxy oxygen atoms, O(3) and O(4), of the deprotonated Schiff bases $(L^1)^{2-}$ and $(L^2)^{2-}$ respectively. In complex **1**, two nitrogen atoms, N(3) and N(4), from two terminal thiocyanate ions coordinate with the Zn(2) centre to fulfil its distorted octahedral geometry, whereas in complex **2**, the axial sites of Zn(2), are occupied by a chloride ion, Cl(2), and an oxygen atom, O(7), of a water molecule. The saturated six-membered chelate rings, Zn(1) – N(1) – C(17) – C(18) – C(21) – N(2) {for complex **1**} and Zn(1)–N(1) – C(10) – C(11) – C(14) – N(2) {for complex **2**}, assume chair conformations with puckering parameters,[53] q = 0.530(10) Å, θ = 36.6(9)°, φ = 169.7(17)° and q = 0.571(4) Å, θ = 16.6(3)°, φ = 200.8(12)°, respectively.

### 3.3. IR and electronic spectra

In the IR spectrum of each complex, a distinct band appears around 1625 $cm^{-1}$ has been identified for stretching vibration of azomethine (C═N) group [54]. In complex **1** a sharp band around 2086 $cm^{-1}$ indicates the presence of a terminal thiocyanate group [55,56]. The bands in the range of 2840–2960 $cm^{-1}$ are due to alkyl C—H bond stretching vibrations that are customarily noticed in the IR spectra of both complexes [57]. In the IR spectrum of complex **2**, two distinct bands are observed at 3351 $cm^{-1}$ and 3419 $cm^{-1}$ which can be assigned as O—H stretching vibrations of coordinating water molecule and lattice methanol molecule [58,59].

There are only three bands in the electronic spectra of both

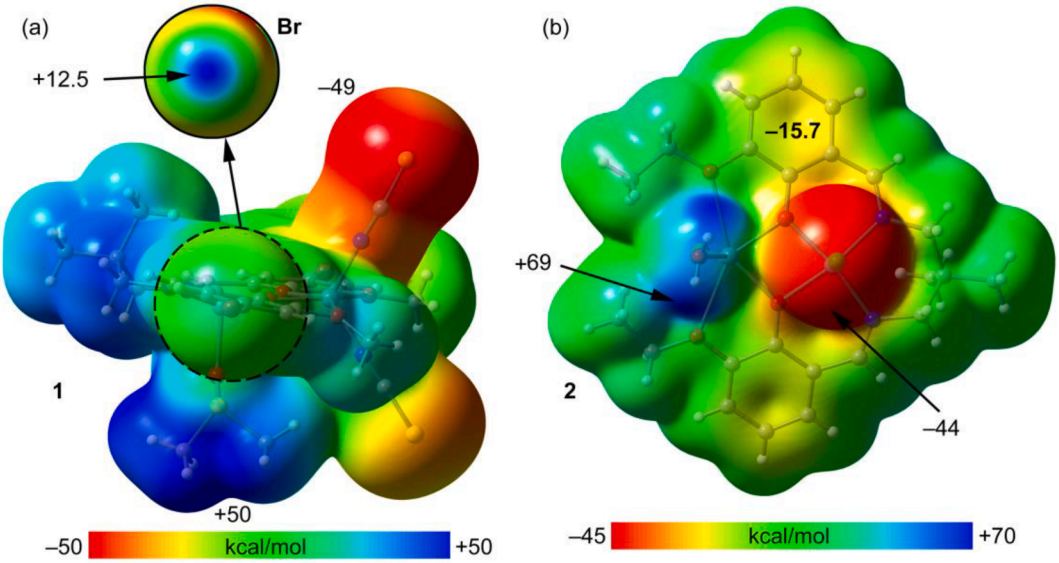


**Fig. 2.** MEP surfaces (isosurface 0.01 a.u.) of complexes **1** (a) and **2** (b). The MEP values at the maximum and minimum are indicated (PBE0-D3/def2-TZVP level of theory). For complex **1**, the MEP around the Br atom has been highlighted using a reduced scale (±13 kcal/mol).

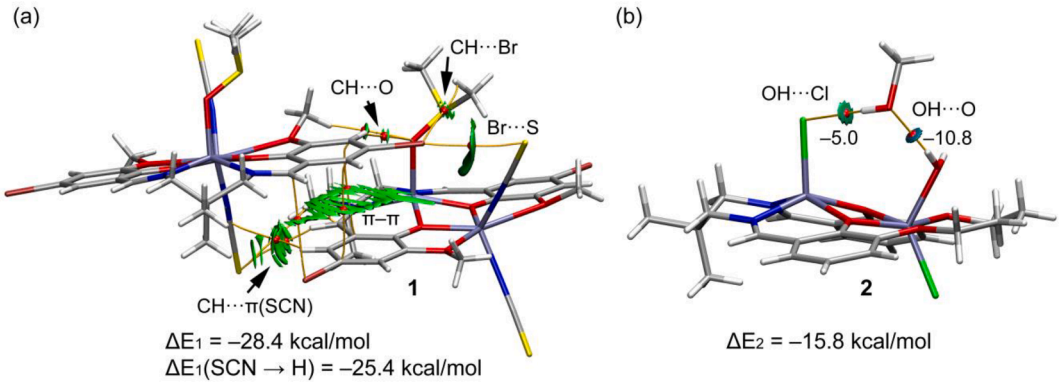


**Fig. 3.** Combined QTAIM (bond CPs in red and bond paths as orange lines) and NCIPlot ($s = 0.5$, cut-off = 0.04 a.u., scale –0.04 a.u. $\leq$ sign($\lambda_2$)$\rho \leq$ 0.04 a.u.) for complexes **1** (a) and **2** (b).(For interpretation of the references to colour in this figure legend, the reader is referred to the web version of this article.)

complexes. Bands at ~ 232 nm and ~ 272 nm may be attributed as π → π* transitions [60]. Bands at ~ 360 nm may be assigned as n → π* transitions. There is no band corresponding to *d–d* electronic transitions, as expected for zinc(II) complexes with $d^{10}$ electronic configuration [61].

### 3.4. Powder X-ray diffraction

The experimental powder XRD patterns of bulk products are in good agreement with simulated XRD patterns (calculated from single crystal X-ray diffraction data) for both complexes. This confirms the purity of the bulk materials. The simulated patterns are calculated from the crystallographic information files (cifs) using the CCDC MERCURY software. The experimental and simulated powder XRD patterns of both complexes have been shown in Figs. S1 and S2, respectively (Supplementary Information, SI).

### 3.5. Theoretical study on solid state supramolecular interactions

In this section, the structure guiding role of some non-covalent interactions observed in the solid state of complexes **1** and **2** is analysed focusing on the different roles of the halogen atoms (electrophilic in **1** and nucleophilic in **2**). First, we, have computed the molecular electrostatic potential (MEP) surfaces of both complexes that are represented in Fig. 2. For complex **1** (Fig. 2a) the minimum MEP (–49 kcal/mol) is located at the thiocyanate ligand (negative belt around the S-atom) and the maximum (+50 kcal/mol) at the H-atoms of the coordinated DMSO molecule. Regarding the bromine atom, it can be observed that a σ-hole appears at the extension of the C–Br bond if a reduced MEP scale (±13 kcal/mol) is used, revealing its electrophilic nature and the anisotropy of the electrostatic potential around this atom (negative belt and positive σ-hole). The MEP surface of complex **2** is represented in Fig. 2b, showing that the maximum and minimum are very close. That is, the minimum (–44 kcal/mol) is located at the chlorido ligand that is coordinated to the Zn(II) occupying the inner $N_2O_2$ compartment. The

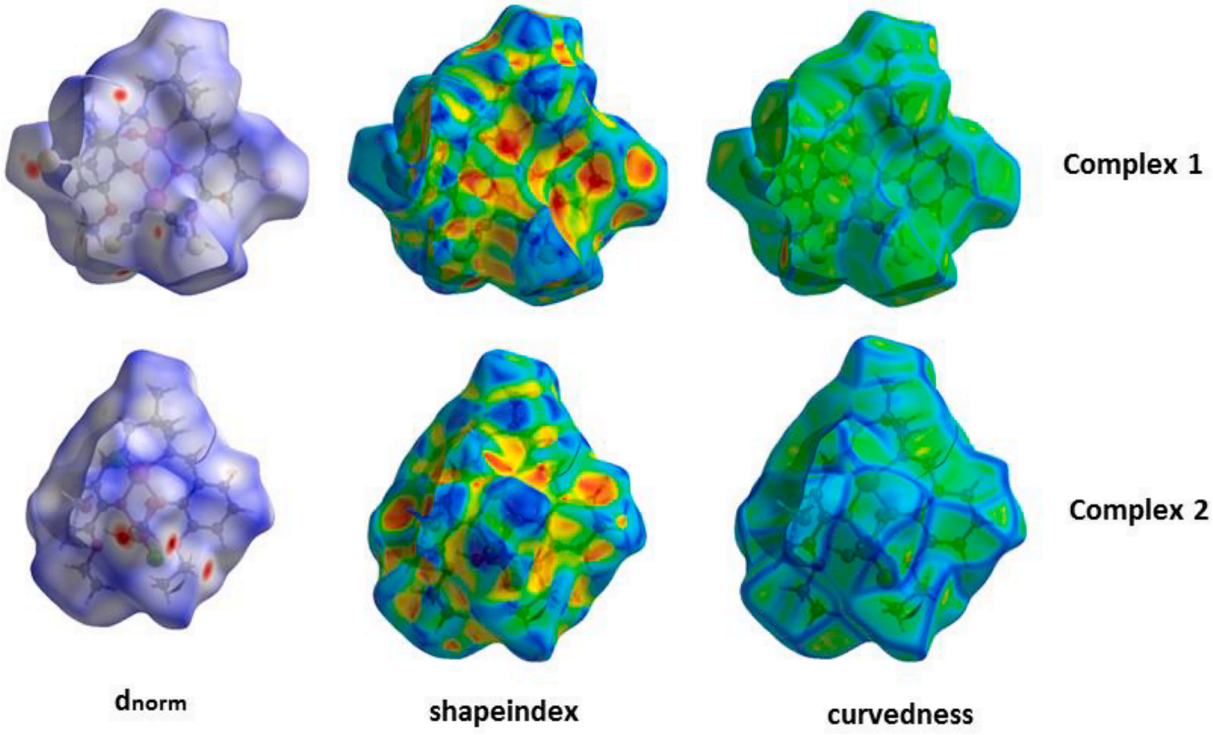


**Fig. 4.** Hirshfeld surfaces mapped with $d_{norm}$(left), shape index (middle), and curvedness (right) for both complexes.

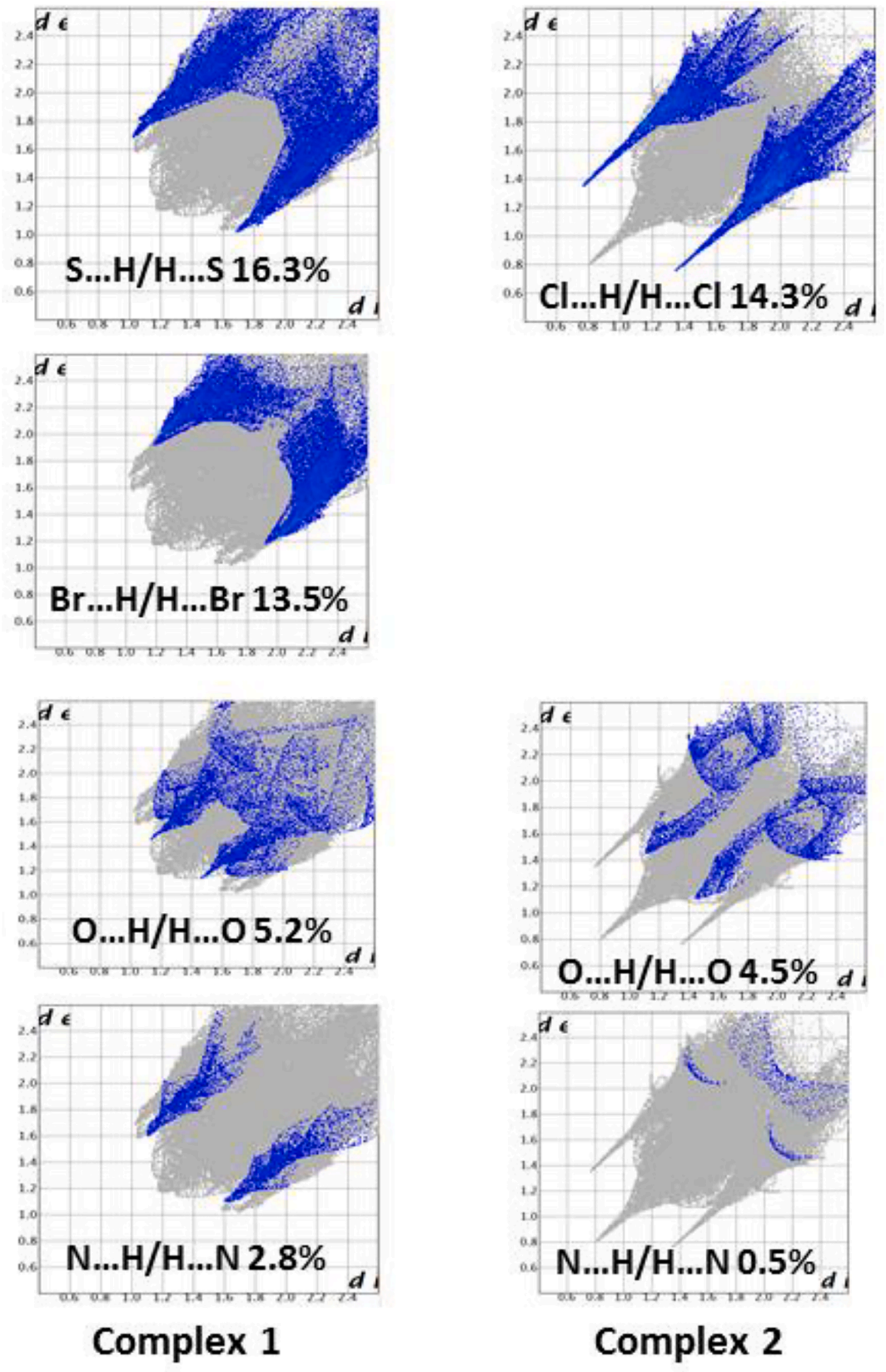


**Fig. 5.** 2D fingerprint plot for both complexes decomposed into different contacts.

**Table 4**
Interaction energies of the molecular pairs in complex **1** given in kJ/mol.

| N | Symmetry Operations | R(Å) | Electron Density | $E_{ele}$ | $E_{pol}$ | $E_{dis}$ | $E_{rep}$ | $E_{tot}$ |
|---|---|---|---|---|---|---|---|---|
| 2 | −x + 1/2, y + 1/2,- z + 1/2 | 11.49 | HF/3-21G | −37.8 | −12.7 | −28.7 | 24.8 | −52.5 |
| 1 | −x, −y, −z | 13.08 | HF/3-21G | 1.1 | −7.8 | −6.6 | 2.2 | −8.0 |
| 2 | −x + 1/2, y + 1/2,- z + 1/2 | 13.70 | HF/3-21G | −8.1 | −2.8 | −16.4 | 5.0 | −20.8 |
| 1 | −x, −y, −z | 12.29 | HF/3-21G | −10.1 | −6.0 | −14.6 | 10.5 | −3.8 |
| 2 | x,y,z | 12.15 | HF/3-21G | 6.1 | −6.5 | −21.5 | 16.8 | −3.8 |
| 2 | x + 1/2, -y + 1/2, z + 1/2 | 8.94 | HF/3-21G | −55.2 | −22.7 | −96.4 | 53.8 | −114.2 |
| 2 | x + 1/2, -y + 1/2, z + 1/2 | 8.86 | HF/3-21G | −49.5 | −31.4 | −53.2 | 29.9 | −94.6 |
| 1 | −x, −y, −z | 12.64 | HF/3-21G | 26.8 | −7.2 | −24.2 | 8.5 | 7.8 |

maximum is located at the H-atoms of the water molecular that is coordinated to the Zn(II) occupying the outer $O_4$ compartment of the Schiff base ligand. The large MEP value (+69 kcal/mol) is due to the enhanced acidity of the water protons upon coordination with the Zn atom. Such arrangement of the ligands and location of the maximum and minimum (close to each other) facilitates the cocrystallization of protic solvent molecules like water or methanol because they are able to interact with both the MEP maximum and minimum establishing two strong H-bonds since they are good H-bond donors and acceptors. In fact, this is observed in complex **2** which incorporates solvent molecules. This aspect is further commented below.

Fig. 3a shows a dimer extracted from the solid state of complex **1** to exemplify the structure guiding interactions. The QTAIM distribution of bond critical points (CPs, bond spheres) and bond paths combined with the NCIplot index analysis are represented in Fig. 3a, since the combination of both methodologies is useful to reveal interactions in real space and characterize them. The self-assembled π-stacked dimer represented in Fig. 3a shows a large and green isosurface located between both aromatic rings along with several bond CPs and bond paths characterizing the π-π stacking. Moreover, the QTAIM analysis shows three H-atoms of the Schiff base ligands connected to the thiocyanate ligand, disclosing the forming of three C—H···π(SCN) interactions. Interestingly, the combined QTAIM/NCIplot analysis also shows that the Br atom is connected to the S-atom of the thiocyanate ligand, establishing a halogen bonding interaction (HaB), in good agreement with the MEP analysis commented above. Such contact is characterized by the corresponding bond CP, bond path and green isosurface that coincide with the location of the bond CP. The dimerization energy is very large ($\Delta E_1$ = –28.4 kcal/mol) due to the contribution of all interactions. In order to evaluate the contribution of the halogen bonding to the total, we have used a mutated dimer where the thiocyanate ligand has been replaced by a hydrido ligand. As a result, the halogen bonding is not formed and the dimerization energy is reduced to $\Delta E_1(SCN \rightarrow H)$ = –25.4 kcal/mol, thus revealing that the halogen bonding is –3.0 kcal/mol, in line with similar HaBs [62].

As commented above, in complex **2** the role of the halogen atom is different due to its anionic co-ligand nature. Fig. 3b shows the QTAIM/NCIplot analysis of the complex interacting with the co-crystallized solvent molecule that connects the coordinated water and chlorido ligands via two H-bonds. Each one is characterized by a bond CP, bond path and green/blue isosurface. The interaction energy of the solvent molecule with **2** is large ($\Delta E_1$ = –15.8 kcal/mol) in sharp agreement with the MEP surface analysis (see Fig. 2b). The O—H···O bond is stronger (blue NCIplot isosurface) in agreement with the large MEP value at the H-atom. In fact, we have estimated the contribution of each H-bond by using the relative values of the potential energy densities ($V_r$) measured at the bond CPs that characterize the interactions. It has been previously demonstrated that the values of Vr correlate with the strength of the H-bond [63]. As a result the strength of the O—H···O contact is almost twice (–10.8 kcal/mol) the strength of the O—H···Cl, in line with the colour of the NCIplot isosurfaces and the MEP values at the maximum (water) and minimum (chloride) in complex **2** (see Fig. 2b).

### 3.6. Hirshfeld surface analysis

Hirshfeld surface analysis is used to analyze the electronic distribution around the surface of a complex which helps in interpreting and visualizing the non-covalent interactions present in the crystal framework. Hirshfeld surfaces of both complexes have been mapped over $d_{norm}$ (-0.5 to 1.5 Å), shape index (-1.0 to 1.0 Å), and curvedness (-4.0 to 0.4 Å) as shown in Fig. 4. The deep red zones on the $d_{norm}$ Hirshfeld surfaces reveal the positions of strong contacts and interactions. The blue and white zone on the surfaces reveals weaker and longer contacts. In complex **1**, S···H/H···S contacts contribute 16.3 % of the overall contacts due to the presence of two thiocyanate co-ligands. Both complexes contain halogen atoms (Br in complex **1** and Cl in complex **2**) which resulted in Br···H/H···Br (13.5 %) and Cl···H/H···Cl (14.3 %) contacts respectively. Other relatively smaller but significant contacts observed are O···H (5.2 % in complex **1** and 4.5 % in complex **2**) and N···H (2.8 % in complex **1** and 0.5 % in complex **2**) contacts. 2D fingerprint plots have been established from $d_e$ and $d_i$, which elaborates the observed contacts/interactions in both complexes (Fig. 5).

### 3.7. Interaction energy calculations

Crystal Explorer 17.5 [64,65] has been used to calculate the

**Table 5**
Interaction energies of the molecular pairs in complex 2 given in kJ/mol.

| N | Symmetry Operations | R(Å) | Electron Density | $E_{ele}$ | $E_{pol}$ | $E_{dis}$ | $E_{rep}$ | $E_{tot}$ |
|---|---|---|---|---|---|---|---|---|
| 1 | – | 4.51 | HF/3-21G | −113.2 | −40.6 | −20.8 | 74.2 | −100.3 |
| 2 | −x, y + 1/2,-z + 1/2 | 10.61 | HF/3-21G | −34.0 | −14.7 | −32.8 | 15.1 | −61.5 |
| 1 | −x, −y, −z | 11.62 | HF/3-21G | 6.1 | −1.4 | −16.1 | 3.0 | −6.7 |
| 1 | – | 9.02 | HF/3-21G | −3.7 | −1.0 | −6.8 | 6.3 | −5.5 |
| 1 | −x, −y, −z | 11.14 | HF/3-21G | −5.5 | −6.8 | −51.9 | 78.2 | 6.7 |
| 2 | x,-y + 1/2,z + 1/2 | 13.83 | HF/3-21G | 0.1 | −0.6 | −14.4 | 6.7 | −7.9 |
| 2 | −x, y + 1/2,-z + 1/2 | 9.13 | HF/3-21G | −42.9 | −21.0 | −57.4 | 33.9 | −81.6 |
| 2 | x,y,z | 13.78 | HF/3-21G | 2.6 | −0.6 | −9.8 | 3.6 | −3.6 |
| 1 | −x,−y,−z | 11.60 | HF/3-21G | −2.0 | −2.4 | −24.3 | 7.5 | −19.4 |
| 2 | x,−y + 1/2,z + 1/2 | 8.23 | HF/3-21G | −59.8 | −23.8 | −28.1 | 82.2 | −35.1 |
| 1 | – | 8.07 | HF/3-21G | −0.9 | −2.4 | −11.2 | 6.1 | −7.5 |
| 1 | −x,−y,−z | 11.13 | HF/3-21G | −3.8 | −2.2 | −19.7 | 3.7 | −20.1 |
| 1 | – | 4.61 | HF/3-21G | −2.3 | −4.3 | −21.6 | 10.3 | −16.2 |

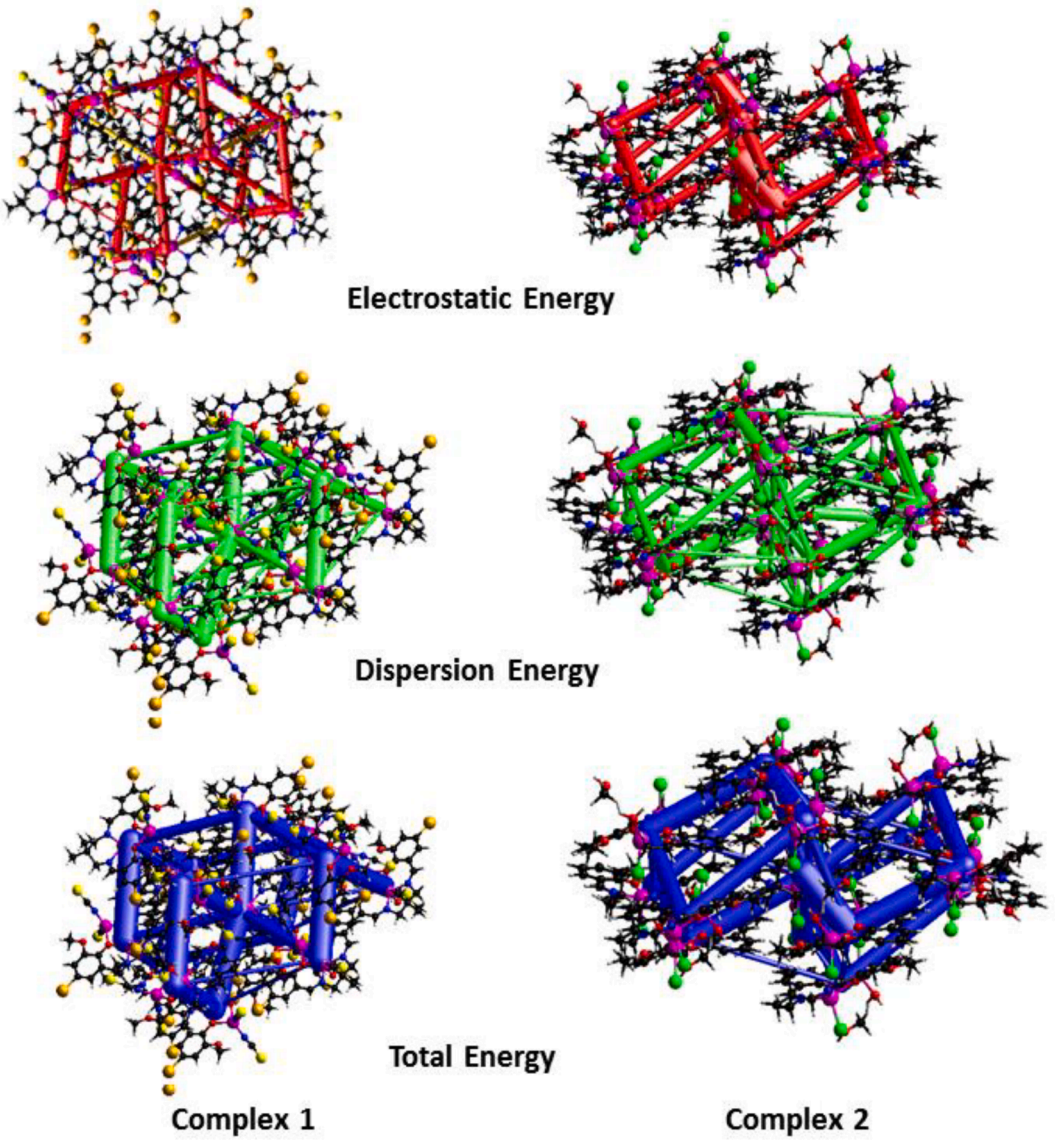


**Fig. 6.** Perspective views of the energy framework for a cluster of molecules in both complexes showing the electrostatic energy (a), dispersion energy (b), and total energy diagrams (c). The cylindrical radius is proportional to the relative strength of the corresponding energies and they were adjusted to the same scale factor of 100 with cut-off values of 10 kJ/mol.

intermolecular energies for both complexes. For a better comparison, the total energies have been decomposed into electrostatic ($E_{ele}$), dispersion ($E_{dis}$), polarization ($E_{pol}$), and exchange-repulsion ($E_{rep}$) energy. The lower basis set HF/6-31G(d,p) has been used for a comparison purpose where a cluster of molecules is generated by applying crystallographic symmetry operations concerning a selected central molecule within the radius of 3.8 Å by default. The total intermolecular energy ($E_{tot}$) is the sum of electrostatic ($E_{ele}$), dispersion ($E_{dis}$), polarization ($E_{pol}$), and exchange-repulsion ($E_{rep}$) energies with scale factors of 1.019, 0.651, 0.901, and 0.811, respectively [66,67]. The calculated interaction energies (kJ/mol) are: –126.7 ($E_{ele}$), –97.1 ($E_{pol}$), –261.6 ($E_{dis}$), 151.5 ($E_{rep}$), and –289.9 ($E_{tot}$) for complex **1** and –259.3 ($E_{ele}$), –121.8 ($E_{pol}$), –314.9 ($E_{dis}$), 330.8 ($E_{rep}$), and –358.7 ($E_{tot}$) for complex **2**. Interaction energies of the molecular pairs in complex **1** and **2** are given in Tables 4 and 5, respectively. In complex **1** dispersion energy is almost double compared to electrostatic energy whereas in complex **2**, the difference between electrostatic and dispersion energy is less which can be predicted from the interactions observed in the crystal packing of both complexes. In complex **1** several halogen bond interactions are observed [Br···π(SCN)] along with weak C—H···π interactions whereas in complex **2** strong hydrogen bond interactions constitutes the crystal packing. These are also observed from the pictorial presentations of energy frameworks shown in Fig. 6.

### 3.8. *Energy frameworks*

The energy frameworks in the Hirshfeld analyses are used to understand the energy difference of intermolecular interactions along with their magnitude [68]. Energies are represented as cylinders between molecular pairs. The radius of the cylinder is directly proportional to the relative strength of the corresponding interaction energy [69]. Energy frameworks are built for $E_{ele}$ (red cylinders), $E_{dis}$ (green cylinders), and $E_{tot}$ (blue cylinders) (Fig. 6) in both complexes. In complex **1** the dispersion energy dominates in every direction of the crystal packing whereas, in complex **2**, electrostatic energy dominates in some directions whereas dispersion energy dominates in other directions which are clear from Fig. 6.

## 4. Conclusions

Two zinc(II) Schiff base complexes have been synthesized and characterized by both experimentally and theoretically. The structural changes have been obtained using unlike coligands and solvents. Different non-covalent interactions observed in their solid state structures have been analysed focusing on the electrophilic (in **1**) or nucleophilic (in **2**) roles of the halogen atoms. MEP surface analyses reveal that the Br atom in complex **1** is electrophilic in nature and take part in halogen bond interactions. In complex **2** as the MEP values in maximum and minimum are very close it facilitates the cocrystallization of protic solvent molecules (like water or methanol).

## CRediT authorship contribution statement

**Tanmoy Basak:** Formal analysis, Investigation, Methodology, Writing – original draft. **Sourav Roy:** Formal analysis, Investigation, Methodology, Writing – original draft, Writing – review & editing, Software. **Snehasis Banerjee:** Formal analysis, Investigation, Methodology, Writing – original draft, Writing – review & editing, Software. **Rosa M. Gomila:** Formal analysis, Investigation, Methodology, Writing – original draft, Writing – review & editing, Software. **Antonio Frontera:** Conceptualization, Data curation, Formal analysis, Funding acquisition, Investigation, Methodology, Project administration, Resources, Software, Supervision, Validation, Visualization, Writing – original draft, Writing – review & editing. **Shouvik Chattopadhyay:** Conceptualization, Data curation, Formal analysis, Funding acquisition, Investigation, Methodology, Project administration, Resources, Software, Supervision, Validation, Visualization, Writing – original draft, Writing – review & editing.

## Declaration of Competing Interest

The authors declare that they have no known competing financial interests or personal relationships that could have appeared to influence the work reported in this paper.

## Data availability

No data was used for the research described in the article.

## Acknowledgements

T.B. thanks the CSIR, India, for awarding a Senior Research Fellowship [Sanction No. 09/096(0861)/2016-EMR-I]. S.R. thanks UGC for a D.S. Kothari Postdoctoral Fellowship. This research was funded by MICIU/AEI of Spain (project PID2020-115637GB-I00 FEDER funds). We thank the "centre de tecnologies de la informació" (CTI) at the University of the Balearic Islands for computational facilities.

## Appendix A. Supplementary data

Supplementary data to this article can be found online at https://doi.org/10.1016/j.poly.2022.116044.

## References

[1] G. Consiglio, S. Failla, P. Finocchiaro, I.P. Oliveri, R. Purrello, S.D. Bella, Inorg. Chem. 49 (2010) 5134–5142.
[2] S. Banerjee, P.-G. Lassahn, C. Janiak, A. Ghosh, Polyhedron 24 (2005) 2963–2971.
[3] P.J. Stang, B. Olenyuk, Acc. Chem. Res. 30 (1997) 502–518.
[4] S. Horiuchi, R. Kumai, Y. Tokura, J. Am. Chem. Soc. 127 (2005) 5010–5011.
[5] S. Roy, M.G.B. Drew, A. Frontera, S. Chattopadhyay, ChemistrySelect 2 (2017) 7880–7887.
[6] M. N. Ahamad, K. Iman, Md K. Raza, M. Kumar, A. Ansari, M. Ahmad, M.Shahid, Bioorg. Chem. 95(2020) 103561.
[7] E.R. Johnson, S. Keinan, P. Mori-Sanchez, J. Contreras-Garcıa, A.J. Cohen, W. Yang, J. Am. Chem. Soc. 132 (2010) 6498–6506.
[8] D.J. McClements, Biotechnol. Adv. 24 (2006) 621–625.
[9] N. Yoshida, H. Oshio, T. Ito, Chem. Commun. (1998) 63–64.
[10] G.A. Bogdanovic, A.S. de Bire, S.D. Zaric, Eur. J. Inorg. Chem. (2002) 1599–1602.
[11] Y.-F. Jiang, C.-J. Xi, Y.-Z. Liu, J.N. Gutierrez, D.C. Lazarte, Eur. J. Inorg. Chem. (2005) 1585–1588.
[12] S. Roy, M.G.B. Drew, A. Bauża, A. Frontera, S. Chattopadhyay, Dalton Trans. 46 (2017) 5384–5397.
[13] P.K. Bhaumik, A. Frontera, S. Chattopadhyay, Inorg. Chim. Acta 515 (2021) 120023–120030.
[14] S. Thakur, M.G.B. Drew, A. Franconetti, A. Frontera, S. Chattopadhyay, RSC Adv. 9 (2019) 35165–35175.
[15] M. Karmakar, A. Frontera, S. Chattopadhyay, CrystEngComm 23 (2021) 1918–1928.
[16] N. Sarkar, M.G.B. Drew, K. Harms, A. Bauzá, A. Frontera, S. Chattopadhyay, CrystEngComm 20 (2018) 1077–1086.
[17] S. Roy, M.G.B. Drew, A. Bauzá, A. Frontera, S. Chattopadhyay, CrystEngComm 20 (2018) 1679–1689.
[18] S. Roy, D. Sutradhar, M.G.B. Drew, S. Chattopadhyay, CrystEngComm 23 (2021) 6724–6735.
[19] S. Kamaal, M. Usman, M. Afzal, A. Alarifi, A.A. RajaDas, P. Lama, M. Ahmad, Polyhedron 193 (2021), 114881.
[20] A. Bhattacharyya, A. Bauzá, A. Frontera, S. Chattopadhyay, Polyhedron 119 (2016) 451–459.
[21] T. Basak, A. Frontera, S. Chattopadhyay, CrystEngComm 22 (2020) 5731–5742.
[22] M. Das, B.N. Ghosh, A. Bauzá, K. Rissanen, A. Frontera, S. Chattopadhyay, RSC Adv. 5 (2015) 73028–73039.
[23] K. Ghosh, K. Harms, A. Bauzá, A. Frontera, S. Chattopadhyay, CrystEngComm 20 (2018) 7281–7292.
[24] S. Khan, A.A. Masum, M.M. Islam, M.G.B. Drew, A. Bauzá, A. Frontera, S. Chattopadhyay, Polyhedron 123 (2017) 334–343.
[25] A. Banerjee, D. Chowdhury, R. M.Gomila and S. Chattopadhyay, Polyhedron, https://doi.org/10.1016/j.poly.2022.115670.
[26] I. Mondal, A. Frontera, S. Chattopadhyay, CrystEngComm 23 (2021) 3391–3397.
[27] S. Mirdya, S. Banerjee, S. Chattopadhyay, CrystEngComm 22 (2020) 237–247.
[28] S. Mirdya, S. Roy, S. Chatterjee, A. Bauzá, A. Frontera, S. Chattopadhyay, Cryst. Growth Des. 19 (2019) 5869–5881.
[29] S. Mirdya, A. Frontera, S. Chattopadhyay, CrystEngComm 21 (2019) 6859–6868.
[30] T. Basak, R.M. Gomila, A. Frontera, S. Chattopadhyay, CrystEngComm 23 (2021) 2703–2710.
[31] M. Karmakar, A. Frontera, S. Chattopadhyay, T.J. Mooibroek, A. Bauzá, Int. J. Mol. Sci. 21 (2020) 7091–7105.
[32] K.T. Mahmudov, M.N. Kopylovich, M.F.C. Guedes da Silva, A.J.L. Pombeiro, Dalton Trans. 46 (2017) 10121–10138.
[33] S. Thakur, M.G.B. Drew, A. Franconetti, A. Frontera, S. Chattopadhyay, RSC Adv. 9 (2019) 4789–4796.
[34] T. Basak, A. Frontera, S. Chattopadhyay, CrystEngComm 33 (2021) 1578–1587.
[35] G.M. Sheldrick, Acta Crystallogr. Sect. C71 (2015) 3–8.
[36] G. M. Sheldrick, SADABS, V2014/5, Software for Empirical Absorption Correction, University of Göttingen, Institute fur Anorganische Chemieder Universitat, Gottingen, Germany, 1999–2003.
[37] C. Adamo, V. Barone, J. Chem. Phys. 110 (1999) 6158–6169.
[38] S. Grimme, J. Antony, S. Ehrlich, H. Krieg, J. Chem. Phys. 132 (2010) 154104–154122.
[39] F. Weigend, Phys. Chem. Chem. Phys. 8 (2006) 1057–1065.
[40] Gaussian 16, Revision A.03, M. J. Frisch, G. W. Trucks, H. B. Schlegel, G. E. Scuseria, M. A. Robb, J. R. Cheeseman, G. Scalmani, V. Barone, G. A. Petersson, H. Nakatsuji, X. Li, M. Caricato, A. V. Marenich, J. Bloino, B. G. Janesko, R. Gomperts, B. Mennucci, H. P. Hratchian, J. V. Ortiz, A. F. Izmaylov, J. L. Sonnenberg, D. Williams-Young, F. Ding, F. Lipparini, F. Egidi, J. Goings, B. Peng, A. Petrone, T. Henderson, D. Ranasinghe, V. G. Zakrzewski, J. Gao, N. Rega, G. Zheng, W. Liang, M. Hada, M. Ehara, K. Toyota, R. Fukuda, J. Hasegawa, M. Ishida, T. Nakajima, Y. Honda, O. Kitao, H. Nakai, T. Vreven, K. Throssell, J. A. Montgomery, Jr., J. E. Peralta, F. Ogliaro, M. J. Bearpark, J. J. Heyd, E. N. Brothers, K. N. Kudin, V. N. Staroverov, T. A. Keith, R. Kobayashi, J. Normand, K. Raghavachari, A. P. Rendell, J. C. Burant, S. S. Iyengar, J. Tomasi, M. Cossi, J. M. Millam, M. Klene, C. Adamo, R. Cammi, J. W. Ochterski, R. L. Martin, K. Morokuma, O. Farkas, J. B. Foresman, D. J. Fox, Gaussian, Inc., Wallingford CT, (2016).
[41] R.F.W. Bader, Chem. Rev. 91 (1991) 893–928.
[42] J. Contreras-Garcia, E.R. Johnson, S. Keinan, R. Chaudret, J.P. Piquemal, D. N. Beratan, W. Yang, J. Chem. Theory Comput. 7 (2011) 625–632.
[43] T. Lu, F. Chen, J. Comput. Chem. 33 (2012) 580–592.
[44] J.W. Humphrey, A. Dalke, K. Schulten, J. Mol. Graph. 14 (1996) 33–38.
[45] R. Yadav, M. Trivedi, G. Kociok-Köhn, R. Prasad, A. Kumar, CrystEngComm 17 (2015) 9175–9184.
[46] M.A. Spackman, D. Jayatilaka, CrystEngComm 11 (2009) 19–32.
[47] J.J. McKinnon, M.A. Spackman, A.S. Mitchell, Acta Crystallogr. Sect. B: Struct. Sci. 60 (2004) 627–668.
[48] M. J. Turner, J. J. McKinnon, S. K. Wolff, D. J. Grimwood, P. R. Spackman, D. Jayatilaka, M. A. Spackman, *CrystalExplorer*. The University of Western Australia. 2017.
[49] M.A. Spackman, J.J. McKinnon, CrystEngComm 4 (2002) 378–392.
[50] A. Parkin, G. Barr, W. Dong, C.J. Gilmore, D. Jayatilaka, J.J. McKinnon, M. A. Spackman, C.C. Wilson, CrystEngComm 9 (2007) 648–652.
[51] T. Basak, A. Frontera, S. Chattopadhyay, RSC Adv. 11 (2021) 30148–30301.
[52] A.W. Addison, T.N. Rao, J. Reedijk, J. van Rijn, G.C. Verschoor, J. Chem, *Soc.* Dalton Trans. (1984) 1349–1356.

[53] D. Cremer, J.A. Pople, J. Am. Chem. Soc. 97 (1975) 1354–1358.
[54] T. Basak, M.G.B. Drew, S. Chattopadhyay, Inorg. Chem. Commun. 98 (2018) 92–98.
[55] T. Basak, C.J. Gomez-Garcia, R.M. Gomila, A. Frontera, S. Chattopadhyay, RSC Adv. 11 (2021) 3315–3323.
[56] S. Roy, M.G.B. Drew, A. Bauzá, A. Frontera, S. Chattopadhyay, Dalton Trans. 46 (2017) 5384–5397.
[57] S. Roy, S. Halder, A. Dey, K. Harms, P.P. Ray, S. Chattopadhyay, New J. Chem. 44 (2020) 1285–1293.
[58] M. Karmakar, T. Basak, S. Chattopadhyay, New J. Chem. 43 (2019) 4432–4443.
[59] S. Roy, T. Dutta, M.G.B. Drew, S. Chattopadhyay, Polyhedron 178 (2020) 114311–114320.
[60] T. Basak, A. Bhattacharyya, M. Das, K. Harms, A. Bauza, A. Frontera, S. Chattopadhyay, ChemistrySelect 2 (2017) 6286–6295.
[61] T. Basak, A. Bhattacharyya, K. Harms, S. Chattopadhyay, Polyhedron 157 (2019) 449–457.
[62] D.F. Mertsalov, R.M. Gomila, V.P. Zaytsev, M.S. Grigoriev, E.V. Nikitina, F. I. Zubkov, A. Frontera Crystals 11 (2021) 1406–1418.
[63] E. Espinosa, E. Molins, C. Lecomte, Chem. Phys. Lett. 285 (1998) 170–173.
[64] P.R. Spackman, M.J. Turner, J.J. McKinnon, S.K. Wolff, D.J. Grimwood, D. Jayatilaka, M.A. Spackman, J. Appl. Cryst. 3 (2021) 1006–1011.
[65] M.J. Turner, S. Grabowsky, D. Jayatilaka, M.A. Spackman, J. Phys. Chem. Lett. 5 (2014) 4249–4255.
[66] C. F. Mackenzie, P. R. Spackman, D.Jayatilaka, M.A. Spackman, IUCrJ4 (2017) 575–587.
[67] R. Gaur, S. Roy, P. Kallem, F. Banat, J. Mol. Struct. 1265 (2022) 133400–133410.
[68] M.J. Turner, S.P. Thomas, M.W. Shi, D. Jayatilaka, M.A. Spackman, Chem. Commun. 51 (2015) 3735–3738.
[69] P.R. Spackman, M.J. Turner, J.J. McKinnon, S.K. Wolff, D.J. Grimwood, D. Jayatilaka, M.A. Spackman, J. Appl. Cryst. 54 (2021) 1006–1011.